Geosci. Instrum. Method. Data Syst. Discuss., 2, 177–204, 2012
www.geosci-instrum-method-data-syst-discuss.net/2/177/2012/
doi:10.5194/gid-2-177-2012


Discussions Geoscientific Instrumentation Methods and Data Systems



# A mobile X-POL weather radar for hydrometeorological applications in the metropolitan area of São Paulo, Brazil

**A. J. Pereira Filho**

Department of Atmospheric Sciences, Institute of Astronomy, Geophysics and Atmospheric Sciences, University of São Paulo, São Paulo, Brazil

Received: 24 April 2012 – Accepted: 30 April 2012 – Published: 23 May 2012

Correspondence to: A. J. Pereira Filho (apereira@model.iag.usp.br)

Published by Copernicus Publications on behalf of the European Geosciences Union.



## Abstract

This paper presents the first mobile X-band dual-polarization Doppler weather radar termed MXPOL operated by the Laboratory of Hydrometeorology (*LABHIDRO*) of the University of São Paulo, São Paulo, Brazil. It is used in graduate and under graduate courses, real time monitoring and nowcasting of severe weather in the Metropolitan Area of São Paulo (MASP). It is one of the first of its kind to be used operationally to provide real time high spatial resolution polarimetric data. MXPOL is an important component of a Hydrometeorological Forecast System (Pereira Filho et al., 2005) for MASP. This manuscript presents some instances of MXPOL polarimetric measurements of weather systems and their respective microphysical, dynamical and boundary layer features that can improve nowcasting.

## 1 Introduction

The Metropolitan Area of São Paulo (MASP) shown in Fig. 3a is within the Alto Tietê Basin where the population, agriculture, industry, commerce, transport and government activities are highly affected by severe weather associated with flash floods and mood slides as well as other damages caused by hail, lightning, wind gusts during the warm season. Heavy pollution in the cold season also poses significant difficulties at MASP.

A trend in weather patterns in the past seven decades has been analyzed. Hourly records indicate an increase of air temperature of 2.1° C, decrease in relative humidity of 7 %, increase in yearly precipitation of 400 mm and anomalies in wind speed and direction (Pereira Filho et al., 2007). In the past decade alone, an annual average of 20 severe weather episodes occurred in MASP, affecting hundreds of flood and mood sliding prone areas.

About 70 % percent of such severe weather events are associated to local circulation induced by topographic and the MASP heat island (Ferreira et al., 2010) during the warm season. The most common local circulation is the sea breeze. The MASP is

about 50 km distant from the Atlantic Ocean (Fig. 1). Major flood episodes occur in mid afternoon hours while the sea breeze front pushes continent ward from SE against prevailing NW winds (approaching cold front), injecting a deeper layer of moisture over the MASP warmer and drier urban boundary layer. Deep thunderstorms develop in a matter of minutes to cause flash floods and other severe weather features. This manuscript will show and example of such flood related event.

An Integrated Hydrometeorological System for the State of São Paulo (SIHESP) was established to mitigate effects of recurrent extreme weather and climate conditions associated to environmental anthropic changes (Pereira Filho et al., 2007) in this very large urban environment. The SIHESP programme implemented a network of automatic weather stations, upgraded two weather radars, establish high performance computing facilities for weather and regional climate prediction and developed the MXPOL weather radar.

Another important component of SIHESP is the use of high-resolution numerical weather prediction based on the Advanced Regional Prediction System-ARPS (Xue et al., 2003). The dynamics and physics of convective systems are explicitly resolved at higher spatial resolution with assimilation of MXPOL polarimetric variables. Timing, location, dimension, intensity and advection of convection cells are very difficult to forecast or even simulate (Weisman et al., 1997; Xue and Martin, 2006). But, fine resolution data assimilation (e.g. Hu et al., 2006a, b) can be done with MXPOL polarimetric measurements to include important mesoscale microphysical and dynamic features of weather system observed in MASP.

This manuscript presents measurements of precipitating systems with MXPOL. It was designed and built to monitor and to nowcasting weather systems over MASP and the Coast region of São Paulo State. Both regions are affected by floods, mud slides, heavy winds, lightning and hail that cause significant social and economical impacts (Pereira Filho et al., 2007). The Hydrometeorological Forecast System (HFS) was developed to upgrade an existing forecast system for MASP. Measurement campaigns with MXPOL were conducted in Eastern São Paulo State in 2007.



The measurement campaigns were meant to verify the performance of MXPOL on clear air mode with few low elevation angles, longer pulse widths and horizontal polarization to measure boundary layer features late in the morning while sea breeze fronts are moving into MASP. Radar measurements of precipitation were performed with eleven or more elevation angles, shorter pulse widths and simultaneous horizontal and vertical polarization.

Reflectivities above 20 dBZ were deemed associated to significant rainfall rates in this manuscript. Measurements were made and raw data archived, processed and displayed with the interactive radar information system (IRIS) developed by SIGMET. The radar antenna was placed pointing vertically during the passage of a cold front with low azimuth rotation, short pulse width, high signal sampling rate, in horizontal and vertical polarization mode. Lightning temporal and spatial distribution from an integrated detection network was compared with concomitant MXPOL polarimetric variables. Measurements of a conventional S-band weather radar (SPWR) were also compared to respective MXPOL ones for checking spatial coherence and rainfall rate spatial distribution.

It is well know X-band radars suffer from attenuation caused by intervening rainfall (Berne et al., 2006). Since the advent of dual polarization X-band weather radars, attenuation may be corrected accordingly (Anagnostou et al., 2006; Gorgucci and Chadrasekar, 2005; Park et al., 2005) and rainfall rates estimated (Matrosov et al., 2002; Anagnostou et al., 2004). The focus of this manuscript is on the original MXPOL measurements of weather systems without any attenuation corrections.

Section 2 describes the main features of MXPOL and its modus operandi. Section 3 describes antenna pattern measurements, ground clutter features over MASP and vertical pointing measurements of light rainfall. Measurements of sea breeze circulation and gust fronts are shown in conjunction to thunderstorm initiation are described in the Sect. 4. Qualitative interpretation of polarization measurements at the leading edge of a vigorous thunderstorm, and microphysical characteristics of a heavy precipitation events are described in the Sect. 5. A summary of the results are presented in Sect. 6.

## 2 Radar system description

MXPOL is a dual polarization X-band radar system that can be switched to single polarization mode. In horizontal-only transmitted mode with longer pulse length, sensitivity of the radar is better than 3 dB when compared to a dual-polarization mode of operation. In the horizontal-only transmitted mode, the dual-channel receiver is capable of measuring both co- and cross-polarized backscattered signals.

A slant 45 degree transmitted mode with short pulse length is used for measuring precipitation. Figure 1 shows the block diagram of MXPOL. The antenna control and signal processing are the SIGMET RCP8 (radar/antenna control processor) and RVP8 (Digital IF Receiver and Signal Processor) units respectively. IRIS is a LINUX based software that controls both RVP8 and RCP8 processes. It also displays real time PPI and RHI scans and generates volume scans.

The measured variables are the corrected reflectivity ($Z$) and raw reflectivity ($Z_T$), radial velocity ($V_r$), spectral width ($W$), differential reflectivity ($Z_{DR}$), differential propagation phase ($\phi_{DP}$), specific differential phase ($K_{DP}$), magnitude ($\rho_{oHV}$) and phase ($\phi_{HV}$) of correlation coefficient of co-polarization horizontal and vertical backscattered signals. In the case of horizontal-only transmit mode only co-polarization channel-based $Z$, $Z_T$, $V_r$, and $W$ are archived by the radar processor.

An additional feature is that the dual-channel receivers can be programmed to record both co- and cross-polarization received signals for estimating linear depolarization ratio and cross correlation coefficient between co- and cross-polarized backscattered signals. The analysis software generates radar products from raw archived polarimetric measurements. It displays measurements in constant elevation and altitude projections and vertical cross sections.

These radar-based products include cloud tops, rainfall accumulation, maximum value profiles, cross-sections, specified horizontal and vertical products, storm motion forecast, storm tracking and forecasting, warning and centroid plotting, vertically integrated liquid water, estimated wind speed and direction.



Table 1 shows MXPOL's antenna parameters: reflector, pedestal, transmitter and receiver. Each parameter was tested as part of the acceptance procedure and performance was found to be satisfactory or better than the manufacturer's specification.

MXPOL includes a six cylinder 180 HP WV Diesel truck, 18 KVA Diesel generator that can sustain one week long operation if necessary, pneumatic suspension, automatic levelling with auxiliary supports for steep terrain, GPS, and wideband Internet communication systems, SIGMET antenna positioning system, microwave power signal generator and meter, and SIGMET automatic calibration software.

The radar system was design and developed in Brazil. Major radar parts such as magnetron, waveguides, duplexers, switches and receivers are from USA; antenna and pedestal parts from Finland and motors and controls from Italy; truck and cabin were developed in Brazil.

## 3 MXPOL data quality

In general, radar measurements are determined by radar receiver characteristics and can be affected by ground clutter. The extent of ground clutter impact on a precipitation measurement depends on antenna side lobes. Also, co-pol antenna beam widths in horizontal and vertical polarization should be matched so differential reflectivity and propagation phase measurements are not biased by strong spatial gradients in precipitation.

The antenna feed and reflector were tested to check the antenna gain and beam width. A test signal microwave power generator at 9.4 GHz at 14 dBm was connected to feed-horn antenna pointing towards the radar reflector a minimum far-field distance. The received signal by the MXPOL antenna was measured by the RVP8 digitizer. The antenna scan was controlled by RCP8 processor and its position recorded. The test feed-horn was aligned to the radar antenna and performed scan in azimuth and elevation for both H and V polarizations.

The antenna beam patterns for both horizontal and vertical polarizations are shown in Fig. 2a and b, respectively. The horizontal polarization azimuth scan yielded HPBW = 0.95° at −3 dB and first sidelobe at −26 dB and, the elevation scan, HPBW = 0.97° at −3 dB and the first sidelobe at −28 dB. These results were within specifications.

MXPOL measurements were made in the west site of MASP (Fig. 3a) during the passage of an eastward moving squall line associated to a cold front on 26 April 2007 (Pereira Filho et al., 2007). Initially, clear air scan mode was performed for three low antenna elevation angles with maximum sensitivity to measure boundary layer and ground returns features.

Figure 3b to h shows 0.6° PPIs of reflectivity ($Z_h$), radial velocity ($V_r$), and spectral width ($W$). Surface winds were from NNW at 3 m s$^{-1}$ and gusting up to 7 m s$^{-1}$ right before the passage of the squall line over São Paulo City. The 0.6° elevation PPI of the reflectivity field is completely contaminated by ground echoes within the MASP. Reflectivity above 60 dBZ are associated to ground echoes from hills, mountains, buildings, towers and other urban structures.

A time animation of such PPIs (not shown) indicated weaker echoes related to fair weather clouds. In early afternoon, no mid to deep clouds were observed. The area of ground echoes (Fig. 3b) is similar in shape to the satellite image (Fig. 3a). The low noisy reflectivity area between 180° and 300° azimuths is the black sector of the cabin of the radar. Figure 3c shows the radial velocity field where zero radial velocities are co-located with MASP. Furthermore, the spectral width (Fig. 3d) were between 0.2 m s$^{-1}$ and 1.4 m s$^{-1}$ at the center and borders of MASP region, respectively. Surface winds were strong and gusting yielded turbulence and mixing of this urban boundary layer rich in particles.

Backscatter characteristics of the horizontally and vertically polarized echoes are similar within the MASP, so $\rho_{oHV}$ was higher (Fig. 3e). Thus, low elevation polarimetric measurements yielded valuable inside to distinguishing weather from ground echoes under clear air conditions over MASP.



Vertically pointing measurements were made with MXPOL during a cold front passage on 22 May 2007. Figure 4 shows a 3-km CAPPI of rainfall rates and respective echo tops estimated with SPWR at 16:16 UTC and the 12:00 UTC sounding at Campo the Marte, São Paulo, a few kilometers east of MXPOL site. The precipitating system was moving northeastward. Rainfall rates less than 40 mm h$^{-1}$ were observed eastward and lower than 2 mm h$^{-1}$ westward with 18 dBZ echo tops between 6 km and 3.5 km in these two regions, respectively.

MXPOL measurements were made at the rear flack of the cold front. The location of MXPOL is indicated in Fig. 4a. The 12:00 UTC sounding indicated a deep moisture layer extending from the surface to about 300 hPa. The wind profile indicates a 145 knot westerly jet around 150 hPa with very small directional shear. Norwest winds at the surface veering with height indicate warm advection on the warm sector of the cold front. The zero degree Celsius isotherm was at 3792 m altitude.

Figure 5 shows vertical profiles from ground level of $Z_h$, $V_r$, $Z_{DR}$ , $W$, $\phi_{DP}$, $K_{DP}$ , and $\rho_{oHV}$ at 15:20 UTC on 22 May 2007. Figure 5a shows the profile of $Z_h$. The altitude of MXPOL was 760 m so heights are changed to altitude by adding 760 m. Clouds tops of 5 dBZ were at 7860 m altitude. The melting layer was 280 m deep between 3940 m and 3660 m. It is in agreement with the higher altitude of the zero degree Celsius given the warming of the lower troposphere by latent heating release. Ice crystals right above the melting layer have $Z_h \sim 20$ dBZ while small drops below the melting layer have $Z_h \sim 25$ dBZ. In the melting layer, $Z_h$ is 34 dBZ.

The vertical velocity profile in Fig 5B indicates speeds between $-1.2 < V_r < -0.5$ m s$^{-1}$ above the melting layer and $-7.0 < V_r < -6.0$ m s$^{-1}$ below. The terminal velocity tends to decrease as the small drops reach the surface. At the melting layer, the terminal velocity increased exponentially from −1.9 to −5.8 m s$^{-1}$. The spectral width profiles in Fig. 5c shows that turbulence is below 0.4 m s$^{-1}$ above the melting layer and between 1.0 m s$^{-1}$ and 1.4 m s$^{-1}$ below it. The profiles of $Z_{DR}$ varies between −0.2 to −0.5 dB. Higher variation of $Z_{DR}$ below 1000 m height is a near-field effect, but above it

between 1.5 to 2.5 km it averages −0.36 dB, a biases since the layer was populated by small drops yielding light rainfall (local observations).

The differential propagation phase shown in Fig. 5e is fairly constant below the melting layer (∼57°) down to 1 km height. It increases at the melting layer and fluctuates around 58° above it. The 1° increase in the differential propagation phase within the melting layer is consistent with Melnikov et al. (2005). The differential phase shown in Fig. 5f is slightly positive from the surface to 6 km height and become negative above it. Finally, the correlation coefficient HV in Fig. 5g shows fairly constant high values (>0.98) below and above the melting layer and significant lower values at the melting layer and close to the cloud top. It also indicates the good quality of MXPOL polarimetric measurements.

## 4 Boundaries and thunderstorm initiation

Figure 6a and b shows 2° PPIs of the reflectivity field at 19:48 UTC and 20:25 UTC on 16 January 2008, respectively. The reflectivity fields were obtained at 5 min time interval and animated to identify fine lines associated to moving boundaries. Figure 6a shows intense convective cells located towards NE of the MXPOL and along the 120° azimuth. Ground echoes (hills, buildings, power lines, etc.) were observed within 30-km range.

A very fine line of reflectivity between −5 dBZ and 10 dBZ at the 30-km range almost perpendicular to 150° azimuth was moving towards MXPOL and associated with the local late afternoon sea breeze front at 19:48 UTC (16:48 LT). The convective cells towards the produced a gust front moving southwestward with reflectivities between −10 dBZ and −5 dBZ virtually parallel to the 120° azimuth. It intercepted the sea breeze front near the 30-km range and 120° azimuth where just to the west an area of echoes between 10 dBZ and 25 dBZ was observed at 19:48 UTC (Fig. 6a).

These two colliding boundaries moved along the sea breeze front. A deep and intense convective cell was observed at 20:25 UTC exactly where the boundaries



collided. The subsequent cells moved along the zipping of the two boundaries. These boundary layer features normally trigger deep convection (Carbone et al., 1997). In this case, the convective cell was predicted more than 30 min before its mature phase.

In several instances, the incoming see breeze interact with the urban heat island by MASP (Fig. 3a) and produces very deep convection with heavy rainfall, gust winds, lightning and hail that cause occasional deaths, damage to property and disruption of economics.

Figure 7 shows 2° PPI of the differential reflectivity $Z_{DR}$ and reflectivity $Z$ at 18:55 UTC (15:55 LT) on 12 February 2008. It shows a well defined sea breeze front moving towards MXPOL from SE. The reflectivity field in Fig. 7b shows ground echoes reflectivities between −10 to 65 dBZ at 45-km range, three convective cells ($-10 < Z < 50$ dBZ) in the far east and the sea breeze front ($-10 < Z < 15$ dBZ). It triggered severe thunderstorms about 30 min after moving over the MASP (not shown).

The differential reflectivity $Z_{DR}$ field (Fig. 7a) shows that the forward part of the sea breeze front is dominated by negative values and, the backward part, by positive values. It suggests that hydrometeors (e.g. insects and shaft) at the forward site of the sea breeze front tend to be oriented vertically as they are lifted and moved backward. Noteworthy, the sea breeze front can not be seen even at very close range. The more intense ground echoes (Fig. 7b) tend to be associated with very low negative $Z_{DR}$.

A final instance of the sea breeze front and its effect on convection over MASP is shown in Fig. 8. It shows 2° PPI of unfiltered reflectivity $Z$ fields at 18:35 UTC, 19:20 UTC and 19:51 UTC on 20 March 2008. Figure 8a shows ground echoes, convective cells at 60° and 180° azimuth and the sea breeze front ($-5 < Z < 25$ dBZ) almost perpendicular to the 150° azimuth close to the 20-km range. It reached the 10-km (Fig. 8b) and 5-km (Fig. 8c) ranges at 19:20 UTC and 19:51 UTC, respectively.

Figure 8c shows intense convective cells parallel to the region where the sea breeze front was moving 75 min earlier. Thus, the detection of the sea breeze front increases the nowcasting lead time in more than 30 min before any significant precipitation is observed. The increase in leading time in relationship to the conventional S-band radar

is crucial for nowcasting flood related events which correspond to 65 % of all flood events during spring and summer.

## 5 MXPOL microphysical characterization of heavy rainfall

The dynamics and microphysics of a squall line measured by MXPOL starting at 19:50 UTC on 26 April 2007 is qualitatively analyzed. The measurements of the most intense region of the squall line are shown in Fig. 9 through a sequence of 2° PPIs of reflectivity $Z_H$ (A); radial velocity $V_R$ (B); spectral width $W$ (C); differential reflectivity $Z_{DR}$ (D); differential propagation phase $\phi_{DP}$ (E); specific differential phase $K_{DP}$ (F); and correlation coefficient $\rho_{OHV}$ (G). The area of high reflectivities near the center of Fig. 9a is associated to radial velocities $V_R \sim 25\,m\,s^{-1}$ (Fig. 9b) and turbulence $W \sim 3\,m\,s^{-1}$ (Fig. 9c), large drops $Z_{DR} \sim 3\,dB$ (Fig. 9d), lower $\phi_{DP} < 100°$ (Fig. 9f) and $K_{DP} < 3°\,km^{-1}$. The correlation coefficient $\rho_{OHV}$ within the precipitating region is between 0.95 and 0.99 and indicates again the good quality of the polarimetric measurements.

The low elevation PPIs of Fig. 9 are passing through the warm layer of the thunderstorms dominated by drops of various sizes as $Z_{DR}$ (Fig. 9d) and $K_{DP}$ (Fig. 9f) fields are positive except where attenuation is more significant as depicted by the circumference in Fig. 9f. It is caused by large rain drops and hail aloft at the leading edge of the squall line. On another research work, to be published elsewhere, attenuation and $Z_{DR}$ bias (Fig. 5d) are corrected by the self-consistent method (Vivekanandan et al., 2003).

Figure 10 shows cross-sections through the squall line where attenuation is more significant. The direction of the cross-section is indicated in Fig. 9a by the line AA. The $Z_h$ cross-section in Fig. 10a shows a slanted core of reflectivities above 45 dBZ from the surface at 30 km range to 8 km altitude and 35 km range. The circumference indicates where $Z_h$ attenuation is the greatest. One might notice that collocated $K_{DP}$ measurements are not as much affected by large drops (Fig. 10f). The elevated core of high reflectivity at the leading edge is where the strongest updrafts (Fig. 10b). Anvils



precede the heaviest rainfall at surface in about 20 km where radial divergence is highest at 9 km altitude (Fig. 10b). Figure 10h shows a photo of the anvil 40 min early as the squall line moved over MXPOL site.

Radial velocities are in general positive. At the rear side of the squall line near the surface $V_R$ is between 10 to $15\,m\,s^{-1}$. The maximum radial velocities are in the anvil region ($\sim 25\,m\,s^{-1}$). Radial convergence is highest at 2 km altitude and at 35 km range. Radial divergence signatures are apparent near the overshooting dome and at the base of the anvil. The spectral width in Fig. 10c shows that the turbulence is higher near the main updraft and at the anvil and lower at the rear of the squall line.

The differential reflectivity (Fig. 10d) is above 3.5 dB near region of highest reflectivity at the surface at 35 km range. A core of high negative value ($< -3.5$ dB) is at the leading edge of the squall line from 2 to 5 km altitude and 33 to 40 km range. Apparently, drops quickly increase in mass at the leading edge of the storm as they move upwards on a strong updraft where the relative horizontal vorticity is negative (Fig. 10c) centered at 2 km altitude and 33 km range. $Z_{DR}$ is zero at 31 km range and 3 km altitude which suggests the presence of hail (circumference in Fig. 10d).

The differential propagation phase, the specific differential phase and correlation HV are shown in Fig. 10e, f and g, respectively. At the leading edge of the squall line $Z_{DR}$ is negative, $\phi_{DP}$ and $K_{DP}$ are highly positive while $Z_H$ and $\rho_{oHV}$ are fairly low and turbulence is relatively high. These inconsistent features are due to severe attenuation which limits rainfall quantification based on reflectivity. In this instance, $K_{DP}$ is less affected by large drops and might result in better rainfall rate estimation.

On the other end at the rear side of the squall line, $Z_{DR}$ is negative, $\phi_{DP}$ is positive and $K_{DP}$ negative or close to zero and $Z_H \rho_{oHV}$ are low and turbulence is lower. These features suggest a mixture of hydrometeors with different shapes coexist within the region of significantly negative $Z_{DR}$, most probably graupel and ice crystals are being brought down by turbulent eddies and mixed with small droplets at the rear of the thunderstorm.

Pockets of negative $K_{DP}$ between 6 km and 10 km altitude at 10 km, 25 km and 38 km range altitude indicate the presence of ice crystals oriented vertically perhaps by the cloud electric field. Lighting strikes (not shown) were more recurrent near the leading edge of the thunderstorms. That might be useful for nowcasting light strikes in thunderstorms electrically charged.

## 6 Summary

MXPOL was designed and built for heavy duty use. The system was tested on various weather and landscape conditions (e.g. thunderstorms overhead, dirty roads and steep terrain). The power generator fuel autonomy allows its use on remote areas. Furthermore, its communication system based on cell phone technology, though limited can be quite useful to transfer products to remote distances.

MXPOL is a important technical and scientific advancement for radar meteorology in Brazil. It is the first of its kind to provide near real time polarimetric data and products for operational use to monitor and to nowcasting severe weather events in MASP. The dual polarization measurements allow better rainfall estimation. Given its greater sensitivity and dynamic range, MXPOL detects the early development of convection and moving boundaries. The mobility and autonomous operating features of MXPOL makes it an important tool for experiments where infrastructure is limited.

The examples of MXPOL polarimetric measurements presented in this work reveal characteristics of tropical weather systems with high spatial and temporal resolution. MXPOL detected boundary layer circulation and shallow convection up to 60 km in range, convergence, divergence, vorticity and turbulence within cloud systems and advection signatures (not shown), cold and warm microphysics, the melting layer and the precursor to lightning. Limited comparisons suggest MXPOL reflectivity measurements are consistent with SPWR measurements though in some instance severely attenuated by heavy rainfall and hail. The auxiliary in situ measurements from a lightning network,



rain gages and soundings are being used for microphysical retrievals (Vivekanandan et al., 1998; Gorgucci et al., 2008; Spek at al., 2008) with MXPOL measurements.

MXPOL is the first Brazilian X-POL weather radar to be used operationally to deliver real time high spatial resolution polarimetric data for hydrometeorological applications. MXPOL is important for several research studies of cloud microphysics, electricity and dynamics, rainfall quantification and verification, 3-D retrievals, inter-comparison studies, field experiments, mesoscale and synoptic studies, modelling, data assimilation and integration among other research topics of interest. The next steps include implementing the attenuation correction procedure for MXPOL measurements. MXPOL is also an excellent observational tool for under-graduate and graduate courses as well as training programmes. Lastly, MXPOL is also being used on survey studies to implement new radar sites in Brazil.

*Acknowledgements.* The authors are thankful to The Department of Water and Electrical Energy for providing SPWR data. This research and MXPOL were sponsored by The State of São Paulo Research Support Foundation (FAPESP) under granted 13952-2 and by National Research Council – CNPq under grant 304978/2011-6.

## References

Anagnostou, E. N., Anagnostou, M. N., Krajewski, W. F., Kruger, A., and Miriovsky, B. J.: High-resolution rainfall estimation from X-band polarimetric radar measurements, J. Hydrometeor., 5, 110–128, 2004

Anagnostou, M. N., Anagnostou, E. N., and Vivekanandan, J.: Correction for rain path specific and differential attenuation of X-band dual-polarization observations, IEEE T. Geosci. Remote Sens., 44, 2470–2480, 2006.

Bechini, R., Baldini, L., Cremonini, R., and Gorgucci, E.: Differential reflectivity calibration for operational radars, J. Atmos. Ocean. Tech., 25, 1542–1555, 2008.

Berne, A. and Uijlenhoet, R.: Quantitative analysis of X-band weather radar attenuation correction accuracy, Nat. Hazards Earth Syst. Sci., 6, 419–425, doi:10.5194/nhess-6-419-2006, 2006.

Bringi, V. N., Chandrasekar, V., Balakrishnan, N., and Zrníc, D. S.: An examination of propagation effects in rainfall on radar measurements at microwave frequencies, Atmos. Ocean. Tech., 7, 829–840, 1990.

Carbone. R. E., Keenan, T. D., Wilson, J. W., and Hacker, M.: Bounday layer structures and the role of breezes in forcing deep island convection, 28th Conference on Radar Meteorology, Austin Texas, USA, Paper 14A2, 1997.

Caylor, I. J., and Chandrasekar, V.: Time-varying ice crystal orientation in thunderstorms observed with multiparameter radar, IEEE T. Geosci. Remote Sens., 34, 847–858, 1996.

Fereira, M. J., Oliveira, A. P., and Soares, J.: Anthropogenic heat in the City of São Paulo, Brazil, Theor. Appl. Climatol., 104, 43–56, doi:10.1007/s00704-010-0322-7, 2011.

Gorgucci, E. and Chandrasekar, V.: Evaluation of attenuation correction methodology for dual-polarization radars: application to X-band systems, J. Atmos. Ocean. Tech., 22, 1195–1206, 2005.

Gorgucci, E., Chandrasekar, V., and Baldini, L.: Microphysical retrievals from dual-polarization radar measurements at X band, J. Atmos. Ocean. Tech., 25, 1668–1681, 2008.

Hu, M., Xue, M., Gao, J., and Brewster, K.: 3DVAR and cloud analysis with WSR-88D level-II data for the prediction of the Fort Worth, Texas, Tornadic Thunderstorms. Part I: Cloud analysis and its impact, Mon. Weather Rev., 134, 675–798, 2006a.

Hu, M., Xue, M., Gao, J., and Brewster, K.: 3DVAR and cloud analysis with WSR-88D level-II data for the prediction of the Fort Worth, Texas, Tornadic Thunderstorms. Part II: Impact of radial velocity analysis via 3DVAR, Mon. Weather Rev., 134, 699–721, 2006b.

Kim, D.-S., Maki, M., and Lee, D.-I.: Correction of X-band radar reflectivity and differential reflectivity for rain attenuation using differential phase, Atmos. Res., 90, 1–9, 2008.

Klemp, J. B. and Wilhelmson, R. B.: The simulation of three-dimensional convective storm dynamics, J. Atmos. Sci., 35, 1070–1096, 1978.

Matrosov, S. Y., Clark, K. A., Martner, B. E., and Tokay, A.: X-band polarimetric radar measurements of rainfall, J. Appl. Meteor., 41, 941–952, 2002.

Melnikov, A. V., Melnikov, V. M., and Ryzhkov, A. V.: On the differential phase in the melting layer 32nd Conference on Radar Meteorology, Tucson, Arizona, USA, Paper P9R.9, 2005.

Park, S.-G., Maki, M., Iwanami, K., Bringi, V. N., and Chandrasekar, V.: Correction of radar reflectivity and differential reflectivity for rain attenuation at X-band. Part I: Theoretical and empirical basis, J. Atmos. Ocean. Tech., 22, 1621–1632, 2005.





Pereira Filho, A. J., Massambani, O., Hallak, R., and Karam, H.: A hydrometeorological forecast system for the Metropolitan Area of São Paulo, WWRP Workshop on Nowcasting and Very Short Term Forecasting, Toulouse, France, CDROM Proceedings, 2005.

Pereira Filho, A. J., Santos, P. M., Camargo, R., Festa, M., Funari, F. L., Salum, S. T., Oliveira, C. T., Santos, E. M., Lourenço, P. R., da Silva, E. G. W. G., and Fialho, M. A.: Anthropic impacts on the climate of the Metropolitan Area of São Paulo, Bull. of the Brazilian Meteor. Soc., 30, 48–56, ISBN: 1676-014X, 2007 (available in Portuguese).

Spek., A. L. J., Unal, C. M. H., Moisseev, D. N., Russchenberg, H. W. J., Chandrasekar, V., and Dufournet, Y.: A New Technique to Categorize and Retrieve the Microphysical Properties of Ice Particles Above the Melting Layer Using Radar Dual-Polarization Spectral Analysis, J. Atmos. Ocean. Tech., 25, 482–497, 2008.

Testud, J., LeBouar, E., Obligis, E., and Ali-Mehem, M.: The rain profiling algorithm applied to plarimetric weather radar, Atmos. Ocean. Tech., 17, 332–356, 2000.

Vivekanandan, J., Zrnic, D. S., Ellis, S. M., Oye, D., Ryzhkov, A. V., and Straka, J.: Cloud microphysics retrieval using S-band dual-polarization radar measurements, B. Am. Meteorol. Soc., 80, 381–388, 1998.

Vivekanandan, J., Zhang, G., Ellis, S. M., Avery, S., and Rajopadyahya, D.: Radar reflectivity calibration using differential propagation phase measurement, Radio Sci., 38, 1–14, 2003.

Weisman, M. L., Skamarock, W. C., and Klemp, J. B.: The resolution dependence of explicitly modelled convective systems, Mon. Weather Rev., 125, 504–520, 1997.

Wilhelmson, R. B.: The life cycle of a thunderstorm in three dimensions. J. Atmos. Sci., 31, 1629–1561, 1974.

Xue, M. and Martin, W. J.: A high-resolution modelling study of the 24 May 2002 dryline case during IHOP. Part II: Horizontal Convective Rolls and Convective Initiation, Mon. Weather Rev., 134, 172–191, 2006.

Xue, M., Wang, D.-H., Gao, J., Brewster, K., and Droegemeier, K. K.: The Advanced Regional Prediction System (ARPS), storm-scale numerical weather prediction and aata assimilation, Meteor. Atmos. Phys., 82, 139–170, 2003.

**Table 1.** Main parameters of the MXPOL.

| MXPOL system |
|---|
| **Reflector** |
| Parabolic<br>Diameter 2.44 m<br>Antenna Gain 44 dB<br>HPBW at 3 dB < 1.0° |
| **Pedestal** |
| Azimuth scan 0 to 360°<br>Elevation scan 0 to 90°<br>Maximum scan 36° $s^{-1}$ Pointing imprecision <0.1° |
| **Transmitter** |
| Magnetron<br>Frequency 9.4 GHz<br>Peak power 80 KW<br>Pulse modulation<br>PRF 500 to 5000 Hz<br>Pulse width 0.2 to 2 µs<br>Linear polarization (H, V) simultaneous<br>Solid state modulator<br>Duty cycle 0.001 |
| **Reception** |
| Two digital channels (H, V)<br>Radar Noise Figure < 2.5 dB<br>Dynamic range (H, V) > 80 dB<br>ADC 14 bits<br>Local oscillator DAFC<br>MDS (H, V) −113 dBm at 2 µs |



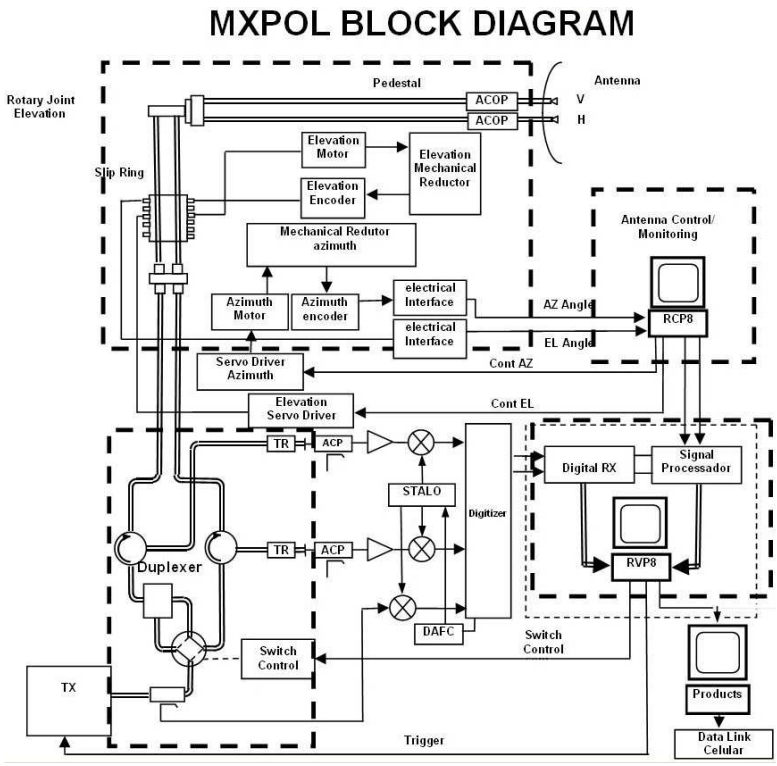


**Fig. 1.** Block diagram of the MXPOL weather radar.

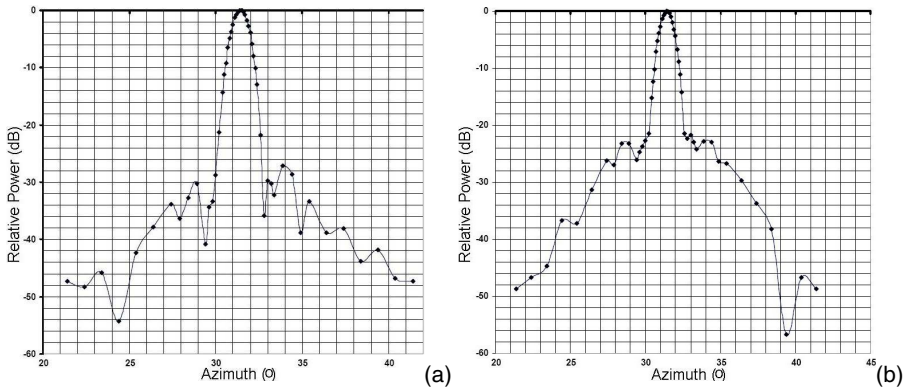


**Fig. 2.** Antenna diagram of the MXPOL transmission and reception of azimuthal scanning of horizontal **(a)** and vertical **(b)** polarizations.





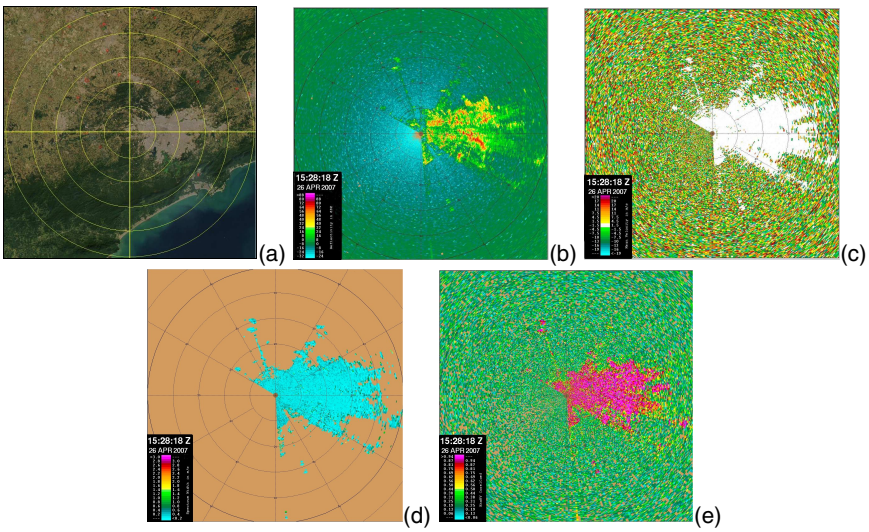


**Fig. 3. (a)** ACQUA/MODIS image of Eastern São Paulo State on 20 July 2003. The cross indicates the MXPOL site (23°32.2′ S; 46°52.8′ W) in Barueri City, São Paulo, Brazil, on 26 April 2007. The large brown area east of the MXPOL site is the MASP. Concentric circumferences spaced every 20 km. Image source: http://visibleearth.nasa.gov/. PPI at 0.6° elevation of reflectivity – $Z_h$ **(b)**, radial velocity – $V_r$ **(c)**, spectral width – $W$ **(d)**, and correlation coefficient VH – $\rho_{oHV}$ **(e)** obtained with MXPOL at 15:28 UTC on 26 April 2007. Ranges, directions and color scales are indicated in each PPI.

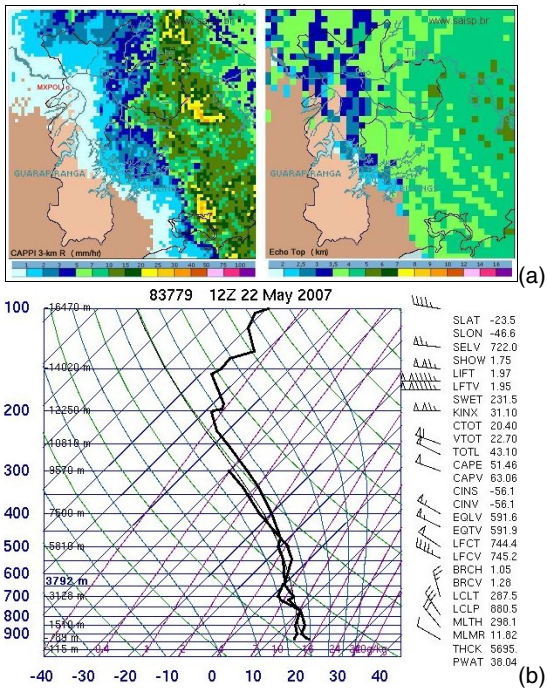


**Fig. 4.** CAPPI of rainfall rates at 3-km altitude (left) and echo tops (right) with 1 × 1-km horizontal resolution estimated with the São Paulo Weather Radar (SPWR) at 16:16 UTC **(a)** and the 12:00 UTC sounding at station 83 779 in São Paulo City **(b)** on 22 May 2007. It is indicated the site (23°33.4′ S; 46°44.1′ W) of the MXPOL **(a)** during the event.





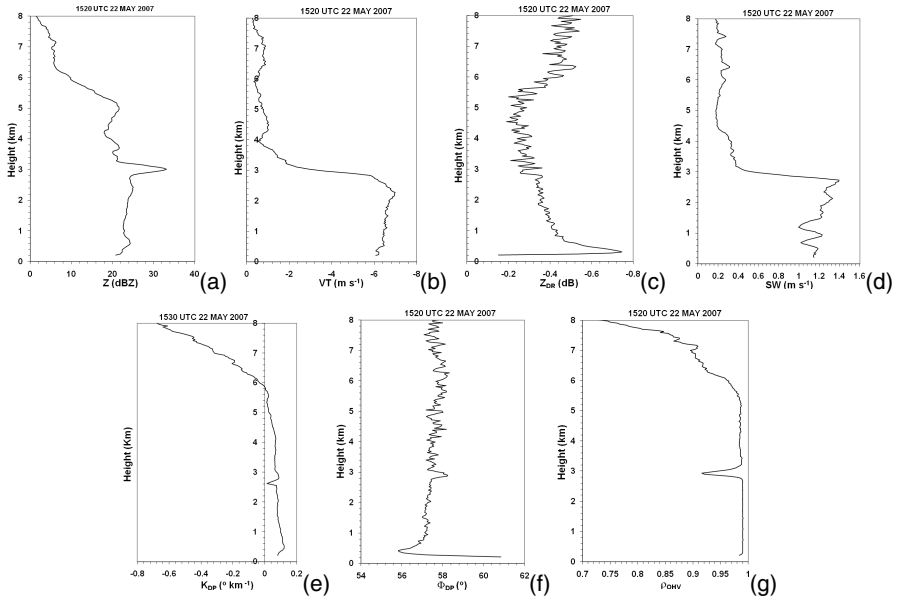


**Fig. 5.** Vertical profiles of reflectivity – $Z_h$ **(a)**, radial velocity – $V_r$ **(b)**, spectral width – $W$ **(c)**, differential reflectivity – $Z_{DR}$ **(d)**, differential propagation phase – $\phi_{DP}$ **(e)**, specific differential phase – $K_{DP}$ **(f)** and correlation coefficient VH – $\rho_{oHV}$ **(g)** obtained with MXPOL at 15:30 UTC on 22 May 2007. Full clockwise antenna scan (6.0° $s^{-1}$) at 90° elevation for pulse width = 0.2 µs, PRF = 1000 Hz and 256 samples, $\Delta z$ = 35.

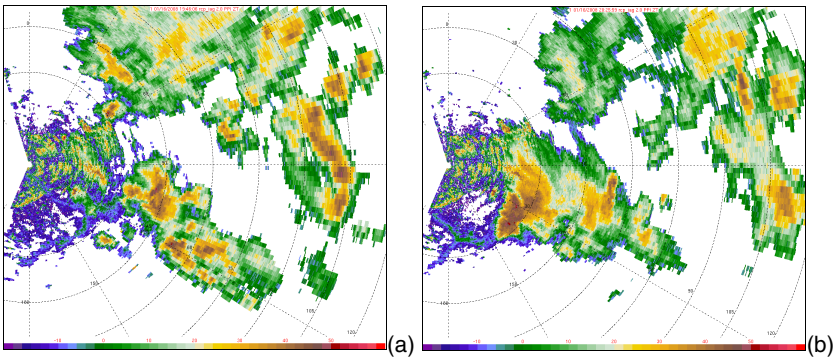

**Fig. 6.** 2° PPI of reflectivity ($Z_h$) at 19:46 UTC **(a)** and 20:25 UTC **(b)** obtained with MXPOL on 16 January 2008. Colour scale is indicated.





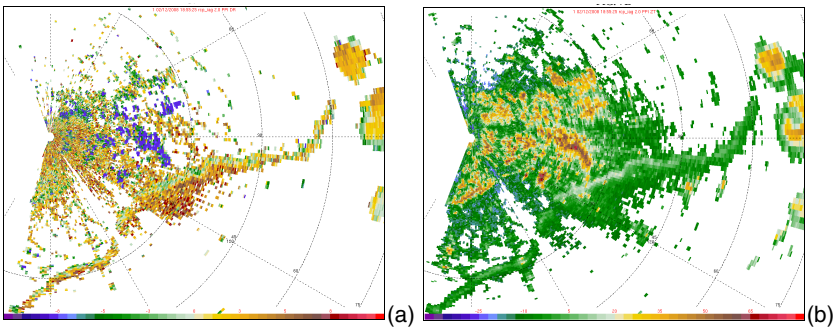

**Fig. 7.** 2° PPI of reflectivity differential reflectivity – $Z_{DR}$ **(a)** and reflectivity – $Z_h$ **(b)** obtained with MXPOL at 18:55 UTC on 16 January 2008. Colour scales are indicated.

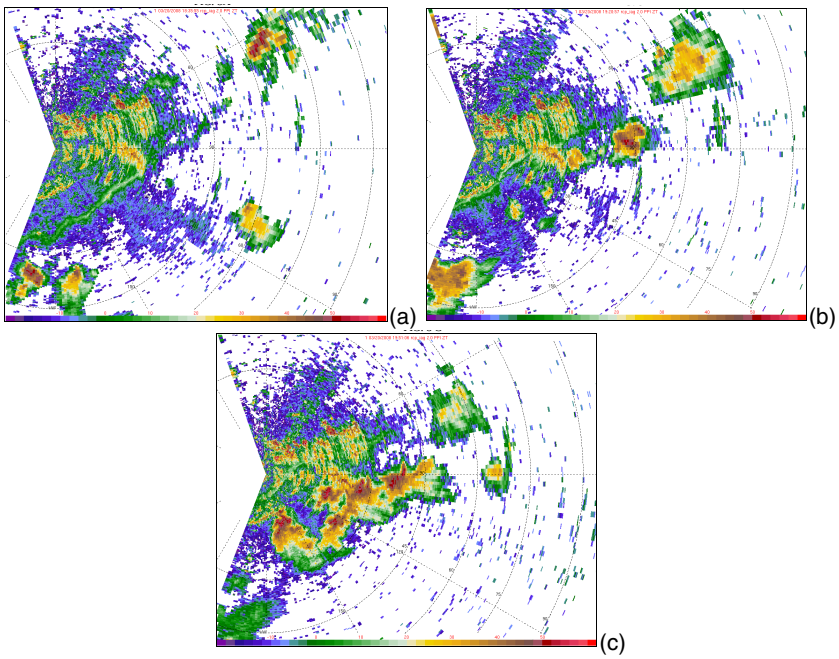


**Fig. 8.** 2° PPI of reflectivity ($Z$) at 18:35 UTC **(a)**, 19:20 UTC **(b)** and 1951 **(c)** obtained with MXPOL on 20 March 2008. Colour scale is indicated.





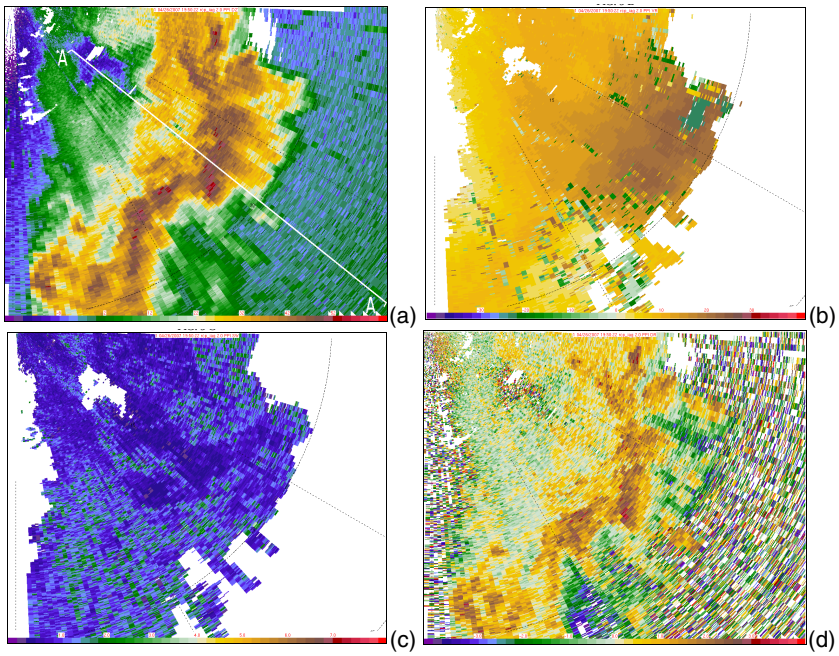


**Fig. 9.** 2° PPI of reflectivity – $Z_h$ **(a)**, radial velocity – $V_r$ **(b)**, spectral width – $W$ **(c)**, differential reflectivity – $Z_{DR}$ **(d)**, differential propagation phase – $\phi_{DP}$ **(e)**, specific differential phase – $K_{DP}$ **(f)** and correlation coefficient VH – $\rho_{oHV}$ **(g)** obtained with MXPOL at 19:50 UTC on 26 April 2007. Colour scales are indicated.

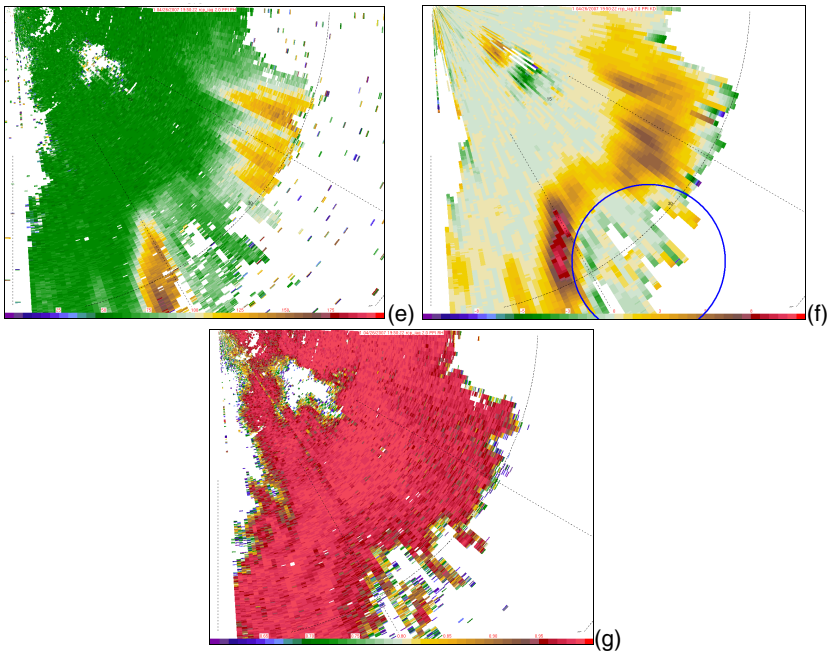


**Fig. 9.** Continued.





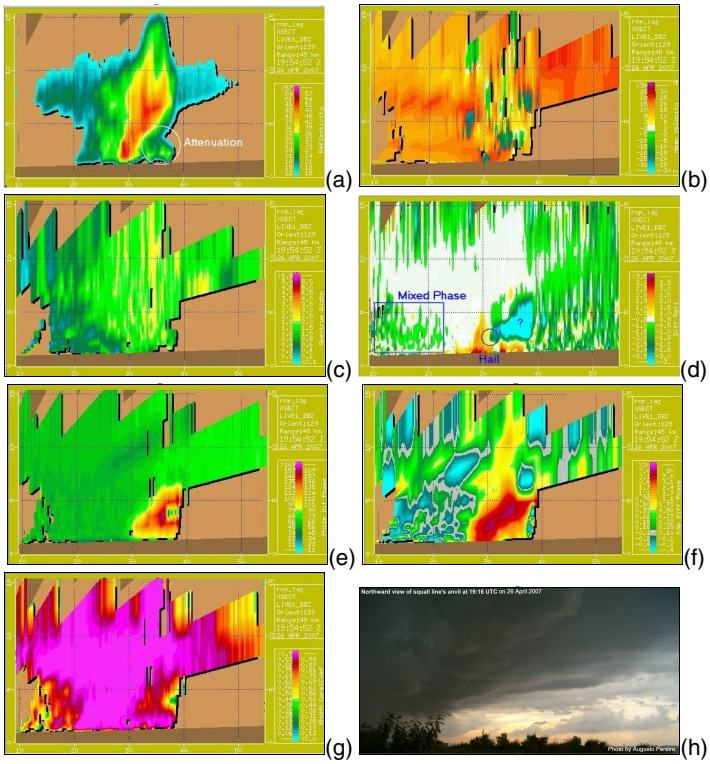


**Fig. 10.** NW-SE cross-sections of reflectivity – $Z_h$ **(a)**, radial velocity – $V_r$ **(b)**, spectral width – $W$ **(c)**, differential reflectivity – $Z_{DR}$ **(d)**, differential propagation phase – $\phi_{DP}$ **(e)**, specific differential phase – $K_{DP}$ **(f)** and correlation coefficient VH – $\rho_{oHV}$ **(g)** obtained with MXPOL at 19:54 UTC on 26 April 2007. Colour scales are indicated in each cross-section. The photo of the anvil of the squall line **(h)** was taken looking Northward from MXPOL site at 19:16 UTC on 26 April 2007.